Sliding Mode PWM-Direct Torque Controlled Induction Motor Drive with Kalman Filtration of Estimated Load

Hau Huu VO[1], *Dat Vinh Phat TRAN*[2], *Tri Quang THIEU*[2], *Anh Tuan LE*[2], *Chau Si Thien DONG*[1,*], *Pavel BRANDSTETTER*[3]

[1]Modeling Evolutionary Algorithms Simulation and Artificial Intelligence, Faculty of Electrical and Electronics Engineering, Ton Duc Thang University, Ho Chi Minh City, Vietnam
[2]Faculty of Electrical and Electronics Engineering, Ton Duc Thang University, Ho Chi Minh City, Vietnam
[3]Faculty of Electrical Engineering and Computer Science, VSB–Technical University of Ostrava, Czech Republic

*Corresponding Author: Chau Si Thien DONG (Email: dongsithienchau@tdtu.edu.vn)
(Received: 18-Sep-2021; accepted: 23-Nov-2021; published: 31-Dec-2021)
DOI: http://dx.doi.org/10.55579/jaec.202154.342

Abstract. *The paper presents an application of sliding mode controller and Kalman Filter (KF-SMC) in speed control of pulse-width-modulation direct torque controlled induction motor drive. Performance of the direct torque control (DTC) is degraded by uncertainty of stator resistance. In order to increase robustness of controlled system to the uncertainty, sliding mode controller (SMC) is utilized to replace proportional-integral (PI) speed controller in conventional DTC drive structure. Computation of SMC requires estimation of load, and Kalman Filter is integrated to reduce noise in load estimation and chattering-phenomenon in speed response. Simulations are carried out at different reference speeds in wide-range noises of stator resistance. Indices including ITAE, settling time, overshoot and undershoot are employed to compare performance of drive structures. Results confirmed the desired characteristics of the proposed drive structure.*

Keywords

Induction motor drive, direct torque control, sliding mode control, load estimation, Kalman filter.

Nomenclature

p	number of pole pairs
R_s	stator resistance
R_r	rotor resistance
L_s	stator inductance
L_r	rotor inductance
L_m	magnetizing inductance
σ	total leakage constant
T_r	rotor time constant
J_m	moment of inertia
$\overline{\mathbf{u}}_s$	stator voltage vector
$\overline{\mathbf{u}}_s^*$	reference stator voltage vector
$u_{s\alpha}, u_{s\beta}$	components of stator voltage vector in stator coordinate system $[\alpha, \beta]$
$u_{s\alpha}^*, u_{s\beta}^*$	components of reference stator voltage vector in stator coordinate system $[\alpha, \beta]$

Nomenclature

u_{sx}^*, u_{sy}^*	components of reference stator voltage vector in stator flux coordinate system $[\alpha, \beta]$
$\bar{\mathbf{i}}_s$	stator current vector
i_{sa}, i_{sb}	phase-a, phase-b stator currents
$i_{s\alpha}, i_{s\beta}$	components of stator current vector in stator coordinate system $[\alpha, \beta]$
$\hat{i}_{s\alpha}, \hat{i}_{s\beta}$	Kalman filtered values of $i_{s\alpha}, i_{s\beta}$
γ	orienting angle
$\hat{\gamma}$	estimated orienting angle
$\overline{\boldsymbol{\psi}_s}$	stator flux vector
$\psi_{s\alpha}, \psi_{s\beta}$	components of stator flux vector in stator coordinate system $[\alpha, \beta]$
$\hat{\psi}_{s\alpha}, \hat{\psi}_{s\beta}$	estimated values of $\psi_{s\alpha}, \psi_{s\beta}$
ψ_s	stator flux vector magnitude
$\hat{\psi}_s$	estimated stator flux vector magnitude
ψ_s^*	reference stator flux magnitude
$\overline{\boldsymbol{\psi}_r}$	rotor flux vector
$\psi_{r\alpha}, \psi_{r\beta}$	components of rotor flux vector in stator coordinate system $[\alpha, \beta]$
T_e	motor torque
$\hat{T}_e$	estimated motor torque
T_e^*	reference motor torque
T_L	load torque
T_{EL}	estimated load torque
$\hat{T}_{EL}$	Kalman filtered value of estimated load torque
T_e^*	reference motor torque
ω_r	rotor speed
ω_m	mechanical speed

1. Introduction

High-performance vector control (VC) strategy in induction motor (IM) drives [1]-[3] can be replaced with pulse-width-modulation (PWM) integrated direct torque control (DTC) strategy [4]-[6]. Parameter tuning, stability analysis and design of proportional-integral (PI) or proportional-integral-derivative (PID) controllers require complicated techniques [7]-[10]. PI and PID controller tuning rules in tabular form are employed in various process models [7]. A set theory-based technique is utilized to obtain robust stability range of PI controller in interval systems [8]. Parameters of a fractional order PID controller are designed to reduce harmonics and noises in IM [9]. In order to obtain good response, and appropriate load disturbance rejection, parameters tuning of the controller is computed by fractional calculus [10].

Several methods for tuning PI or PID controllers are based on intelligent or bio-inspired techniques [11]-[14]. Whale optimization algorithm brings high performance for optimization of PID controller in a DC-DC buck converter [11]. Particle swarm optimization (PSO) provides shorter settling time and lower peak values in PID controlled liquid level system [12]. Combination of neural network and fuzzy logic reduces the time of accommodation, the steady-state error and simultaneously compensate uncertainty in system parameters [13]. Two meta-heuristics method-genetic algorithm and PSO are utilized to adjust coefficients of a Gaussian adaptive PID controller in a DC-DC buck converter.

In order to deal with parameter uncertainty and system disturbances in IM drives, robust control techniques can be selected [15]-[18]. In [15], the optimal preview control theory is utilized, and the robustness is tested via changes of rotor resistance and load torque. The state variable aggregation method is employed in design of VC strategy for the nonlinear model of IM [16]. In order to obtain robustness to the changes of stator and rotor resistances, an input-output feedback linearization control technique is applied [17]. Linear matrix inequality-based state feedback design is carried out in case of system disturbances and parameter uncertainties [18]. One particular method to robust controller design is the sliding mode control (SMC) technique [19].

Variations of SMC are applied in scientific and engineering problems [20]-[25]. Stability analysis and control synthesis of crowd dynamics models are implemented by nonlinear SMC [20]. Double integral SMC is employed for tracking maximum power point of a photovoltaic system [21]. The SMC with a stochastic sliding mode surface is used to stabilize singular Markovian systems with Brownian motion [22]. The digital SMC is designed for the discretized model of the

piezoelectric actuator [23]. The discrete-time two-dimensional SMC is handled for Fornasini-Marchesini systems that are distorted by exogenous nonlinear disturbances [24]. For field of IM drives, SMC is also widely utilized [25]-[28]. A sigmoid function and an adaptive gain are used to eliminate chattering for an IM drive with VC [25]. A gain margin technique is employed to attenuate chattering for continuous SMC of IM servo system [26]. In order to achieve total robustness in VC of IM motion control system, a sliding-mode based component is added to take into account disturbances and uncertainties [27]. A second-order SMC is implemented to control the dynamics of the IM with the aim of disturbance rejection and robustness assurance [28]. For simplicity, in the paper, integral SMC technique [25] is chosen to design control signal of DTC-IM drive for robustness to high uncertainty of stator resistance. In order to ensure boundary condition of system's Lyapunov stability and reduce chattering-phenomenon, a load estimation method based on dynamic equation of rotational motion and Kalman filter [6] is utilized. In next section, SMC drive structures for DTC drive are presented. Simulation results and conclusions are respectively given in two last sections.

2. DTC-IM drive with sliding mode speed controller

State-space model [29] of IM in coordinate system $[\alpha, \beta]$ is described by Eqs. (1)-(2):

$$\dot{\mathbf{X}} = \mathbf{AX} + \mathbf{BU} \tag{1}$$

$$\mathbf{Y} = \mathbf{X} \tag{2}$$

where:

$$\mathbf{X} = \begin{bmatrix} \bar{\mathbf{i}}_s & \overline{\boldsymbol{\psi}_r} \end{bmatrix}^{\mathbf{T}}, \mathbf{U} = \bar{\mathbf{u}}_{\mathbf{s}}^{\mathbf{T}} \tag{3}$$

$$\mathbf{A} = \begin{bmatrix} \mathbf{A_{11}} & \mathbf{A_{12}} \\ \mathbf{A_{21}} & \mathbf{A_{22}} \end{bmatrix}, \mathbf{A_{11}} = a_1\mathbf{I} \tag{4}$$

$$\mathbf{A_{12}} = a_2\mathbf{I} - a_3\omega_r\mathbf{J}, \ \mathbf{A_{21}} = \frac{L_m}{T_r}\mathbf{I} \tag{5}$$

$$\mathbf{A_{22}} = -\frac{1}{T_r}\mathbf{I} + \omega_r\mathbf{J}, \mathbf{B} = \begin{bmatrix} \frac{1}{\sigma L_s}\mathbf{I} & 0 \end{bmatrix}^{\mathbf{T}} \tag{6}$$

$$\mathbf{I} = \begin{bmatrix} 1 & 0 \\ 0 & 1 \end{bmatrix}, \mathbf{J} = \begin{bmatrix} 0 & -1 \\ 1 & 0 \end{bmatrix}, \mathbf{0} = \begin{bmatrix} 0 & 0 \\ 0 & 0 \end{bmatrix} \tag{7}$$

$$a_1 = -\frac{L_m^2 R_r + L_r^2 R_s}{\sigma L_s L_r^2}, a_2 = \frac{L_m R_r}{\sigma L_s L_r^2} \tag{8}$$

$$a_3 = \frac{L_m}{\sigma L_s L_r}, T_r = \frac{L_r}{R_r}, \sigma = 1 - \frac{L_m^2}{L_s L_r} \tag{9}$$

Rotor speed is obtained according to Eqs. (10)-(11):

$$T_e = \frac{3}{2}\frac{L_m}{L_r}p(\psi_{r\alpha} i_{s\beta} - \psi_{r\beta} i_{s\alpha}) \tag{10}$$

$$\frac{d\omega_m}{dt} = \frac{T_e - T_L}{J_m}, \quad \omega_r = p\omega_m \tag{11}$$

Figure 1 shows proposed DTC-IM drive structure with sliding mode-based speed controller (SMBSC). Basic quantities of PWM-DTC are expressed by Eqs. (12)-(16):

$$\hat{\psi}_{s\alpha} = \int \left(u_{s\alpha} - \hat{i}_{s\alpha} R_s\right) dt \tag{12}$$

$$\hat{\psi}_{s\beta} = \int \left(u_{s\beta} - \hat{i}_{s\beta} R_s\right) dt \tag{13}$$

$$\hat{\psi}_s = \sqrt{\hat{\psi}_{s\alpha}^2 + \hat{\psi}_{s\beta}^2} \tag{14}$$

$$\hat{\gamma} = \arcsin\left(\hat{\psi}_{s\beta} \Big/ \hat{\psi}_s\right) \tag{15}$$

$$\hat{T}_e = (3p/2)\left(\hat{i}_{s\beta}\hat{\psi}_{s\alpha} - \hat{i}_{s\alpha}\hat{\psi}_{s\beta}\right) \tag{16}$$

Computation process of Kalman Filtered stator current components is described in [6]. For drive structure with SMBSC, design process of reference torque requires load information, and Kalman Filtered load estimation block is added to reduce ripple of estimated load torque.

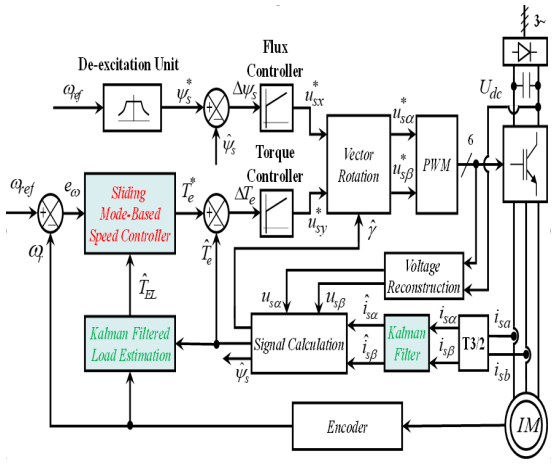

Fig. 1: DTC-IM drive with sliding mode-based speed controller.

In SMBSC design, sliding surface and its time derivative are modified from [25], and expressed by Eqs. (17)-(18):

$$S = \int (\omega_{ref} - \omega_r)dt + k_1(\omega_{ref} - \omega_r) \tag{17}$$

$$\dot{S} = \omega_{ref} - \omega_r + k_1\dot{\omega}_{ref} - k_1\dot{\omega}_r \tag{18}$$

where $k_1 > 0$. Assume that reference torque-output of SMC is equal to real motor torque, time derivative of rotor speed can be computed as Eq. (19):

$$\dot{\omega}_r = p(T_e^* - T_L)/J_m \tag{19}$$

Assume that reference rotor speed is constant, Eq. (18) is rewritten as follows:

$$\dot{S} = \omega_{ref} - \omega_r - k_1 p(T_e^* - T_L)/J_m \tag{20}$$

In order to ensure the stability of the controlled system, the Lyapunov's stability theorem is utilized. Define the Lyapunov function candidate according to Eq. (21):

$$V = S^2/2 \tag{21}$$

Its time derivative is given by Eq. (22):

$$dV/dt = S\dot{S} \tag{22}$$

The controlled system is stable if the term dV/dt is negative. Similarly to [25], we can choose the time derivative of the sliding surface as Eq. (23):

$$\dot{S} = -k_2 sign(S) \tag{23}$$

where $k_2 > 0$. From Eqs. (20), (23), we obtain the SMBSC control law:

$$T_e^* = \frac{J_m}{k_1 p}\left[k_2 sign(S) + e_\omega\right] + T_L \tag{24}$$

However, information of load torque is unknown, so it is considered noise. The Eq. (24) is rewritten:

$$T_e^* = \frac{J_m}{k_1 p}\left[k_2 sign(S) + e_\omega\right] \tag{25}$$

The coefficient k_2 is designed to maintain system stability with control law described in Eq. (25). The Eq. (20) is converted into Eq. (26) thanks to Eq. (25):

$$\dot{S} = -k_2 sign(S) + k_1 p\frac{T_L}{J_m} \tag{26}$$

Assume that load torque is bounded, k_2 is chosen as follows:

$$k_2 = \frac{k_1 p}{J_m} M_L \tag{27}$$

where $M_L > |T_L|$. It is easy to see that the smaller M_L is, the more chattering problem is reduced. So it is necessary to estimate the load torque T_L. Its simple approximation T_{EL} is described by Eq. (28):

$$T_{EL} = \hat{T}_e - \frac{J_m}{p}\dot{\omega}_r \tag{28}$$

Estimated motor torque which is computed by Signal Calculation block (see Fig. 1), can be distorted (see Eqs. (12), (13), (16)) although two stator current components were filtered. Hence, estimated load is also deformed, and it is Kalman filtered according to Eqs. (29)-(36):

$$x_k = x_{k-1} + w_{k-1} \tag{29}$$

$$y_k = x_k + v_k \tag{30}$$

$$\tilde{x}_k = \hat{x}_{k-1} \tag{31}$$

$$\tilde{P}_k = \hat{P}_{k-1} + Q \tag{32}$$

$$\tilde{z}_k = y_k - \tilde{x}_k \tag{33}$$

$$K_k = \tilde{P}_k \Big/ \left(\tilde{P}_k + R\right) \tag{34}$$

$$\hat{x}_k = \tilde{x}_k + K_k \tilde{z}_k \tag{35}$$

$$\hat{P}_k = (1 - K_k)\, \tilde{P}_k \tag{36}$$

where: $x = T_{EL}$: state scalar; w, v: zero-mean Gaussian process, measurement noise scalars with unknown variances Q, R; symbols $\wedge, \sim$ denote estimated, predicted scalars respectively. The component ML in Eq. (27) is chosen as follows:

$$M_L = \max\left(\left|\hat{T}_{EL}(k-1)\right|, \left|\hat{T}_{EL}(k)\right|\right) + \varepsilon \tag{37}$$

where ε is positive and arbitrarily small.

3. Simulation results

In this section, parameters of simulated IM and SVPWM-DTC drive are listed in Tab. 1. Simulations are implemented at reference speeds of 500 rpm, 50 rpm, 5 rpm (see Figs. 2-4) with load jump of 8 Nm at 0.3 s (see Fig. 5). In order to verify theoretical assumptions, stator resistance R_s is assumed to be distorted by zero-mean Gaussian noise with variance of added relative value $\sigma_{R^2} = \{0.1^2, 0.3^2, 0.5^2, 0.7^2, 0.9^2\}$, and vector of stator current components is also considered to be deformed by zero-mean Gaussian noise vectors with covariances $\sigma_{P^2} = \sigma_{M^2} I = 0.3^2 I$ (see [6]).

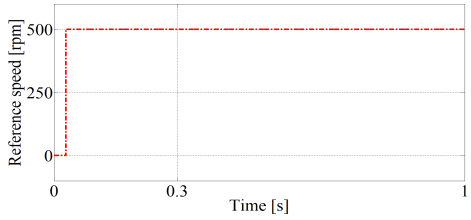

Fig. 2: Reference speed $\omega_{ref} = 500$ rpm.

Performance indices including Integral Time Absolute Error (ITAE), settling times, overshoot and undershoot are utilized to evaluate three drive structures: structure in [6] – PI one, SMC structure in Fig. 1 without Kalman filtration in load estimation – SMC one, SMC struc-

Tab. 1: Parameters of IM and SVPWM-DTC drive.

Parameter	Value
Rated power	2.2 kW
Rated speed	1420 rpm
Rated voltage	230 V/400 V
Rated torque	14.8 Nm
Number of pole pairs	2
Moment of inertia	0.0047 kgm^2
Stator resistance	3.179 W
Stator inductance	0.209 H
Mutual inductance	0.192 H
Rotor resistance	2.118 W
Rotor inductance	0.209 H
Voltage of DC link	540 V
Switching frequency	20 kHz
Limits of output of speed controllers	±14 Nm

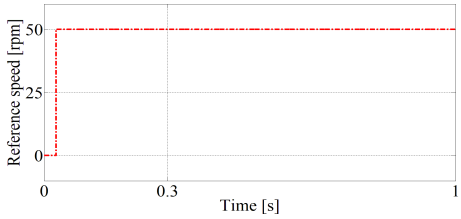

Fig. 3: Reference speed $\omega_{ref} = 50$ rpm.

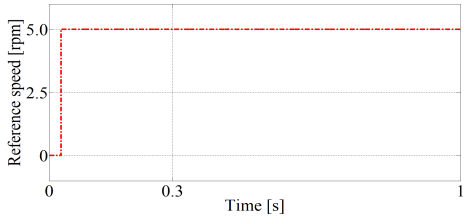

Fig. 4: Reference speed $\omega_{ref} = 5$ rpm.

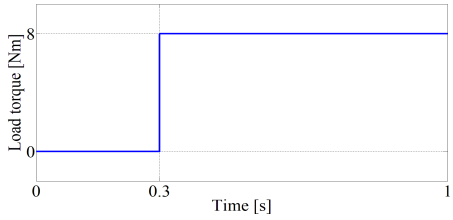

Fig. 5: Load torque with jump of 8 Nm at 0.3 s.

ture in Fig. 1 – KFSMC one. The ITAE index is computed according to Eq. (38):

$$ITAE = \int_0^1 t\,|e_\omega(t)|\,dt \tag{38}$$

Settling times t_{s1} and t_{s2} are respectively searched in durations 0.0 s – 0.3 s (before load activation), and 0.3 s – 1.0 s (after load activation). Overshoot and undershoot are also calculated in two same durations respectively.

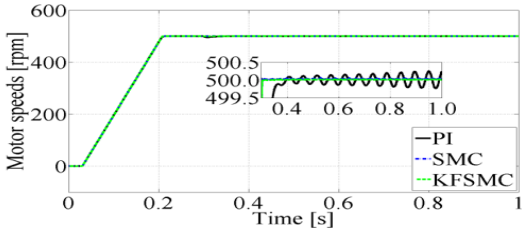

Fig. 6: Motor speeds at $\omega_{ref} = 500$ rpm, $\sigma_{R^2} = 0.1^2$.

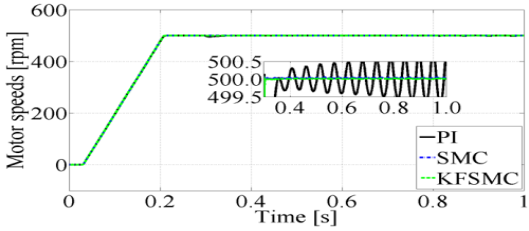

Fig. 7: Motor speeds at $\omega_{ref} = 500$ rpm, $\sigma_{R^2} = 0.3^2$.

Figures 6-20 shows speed responses of 3 structure drives in cases of $\omega_{ref} = \{500, 50, 5\}$, $\sigma_{R^2} = \{0.1^2, 0.3^2, 0.5^2, 0.7^2, 0.9^2\}$. At the same reference speed, after load activation, response for PI structure owns higher oscillation when variance σ_{R^2} is larger, while responses for SMC and KFSMC structures are almost unchanged. Overshoots and undershoots for PI structure are significantly greater than ones for SMC and KFSMC structures, especially at reference speeds of 50 rpm and 5 pm. Tabs. 2-4 respectively list all values of ITAE, overshoot, and undershoot.

In Tab. 2, at $\omega_{ref} = 500$ rpm, ITAE for KFSMC structure is smallest one but difference is not significant, they are 88.48%-97.89% and 99.81%-99.84% of ones for PI and SMC structures respectively. For $\omega_{ref} = 50$ rpm, ratios are respectively 7.85%-28.35% and 75.20%-

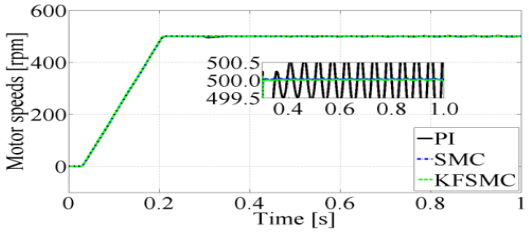

Fig. 8: Motor speeds at $\omega_{ref} = 500$ rpm, $\sigma_{R^2} = 0.5^2$.

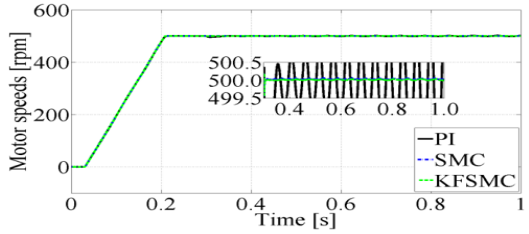

Fig. 9: Motor speeds at $\omega_{ref} = 500$ rpm, $\sigma_{R^2} = 0.7^2$.

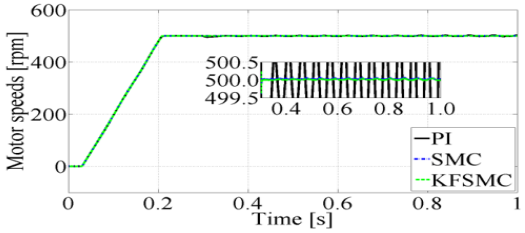

Fig. 10: Motor speeds at $\omega_{ref} = 500$ rpm, $\sigma_{R^2} = 0.9^2$.

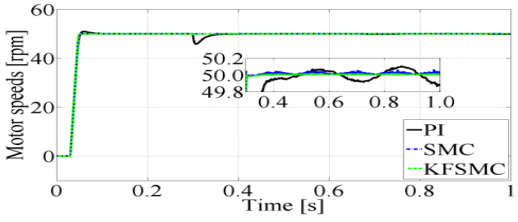

Fig. 11: Motor speeds at $\omega_{ref} = 50$ rpm, $\sigma_{R^2} = 0.1^2$.

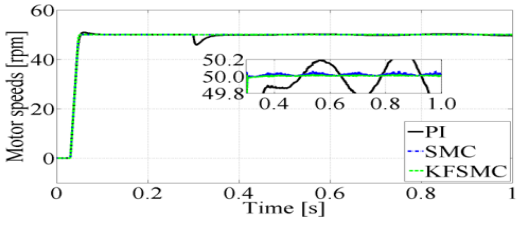

Fig. 12: Motor speeds at $\omega_{ref} = 50$ rpm, $\sigma_{R^2} = 0.3^2$.

76.42%, and in case of $\omega_{ref} = 5$ rpm, values are 2.40%-8.20% and 51.22%-52.88% respec-

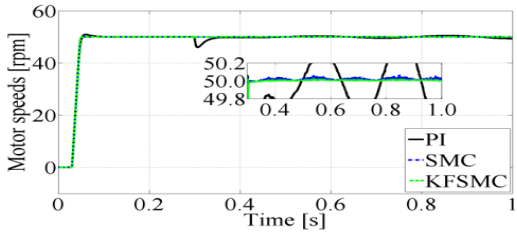

Fig. 13: Motor speeds at $\omega_{ref} = 50$ rpm, $\sigma_{R^2} = 0.5^2$.

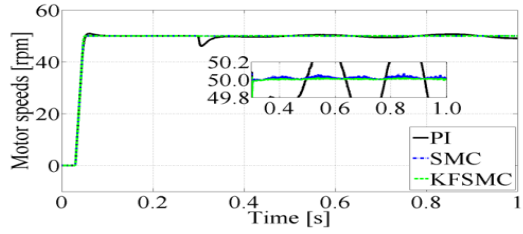

Fig. 14: Motor speeds at $\omega_{ref} = 50$ rpm, $\sigma_{R^2} = 0.7^2$.

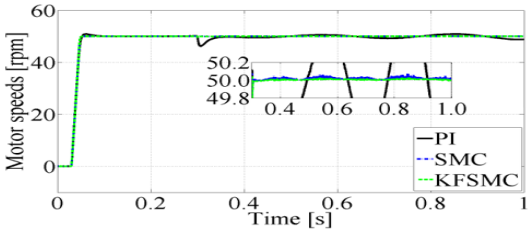

Fig. 15: Motor speeds at $\omega_{ref} = 50$ rpm, $\sigma_{R^2} = 0.9^2$.

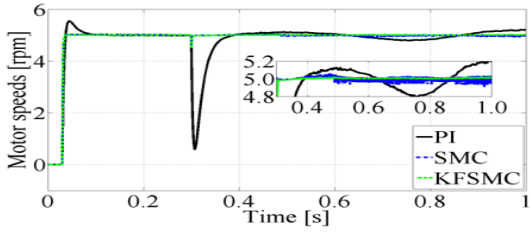

Fig. 16: Motor speeds at $\omega_{ref} = 5$ rpm, $\sigma_{R^2} = 0.1^2$.

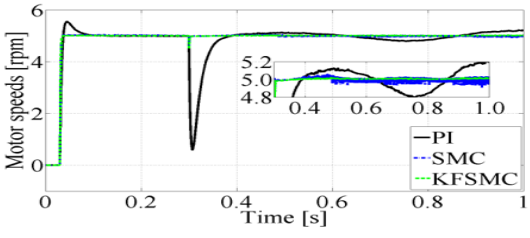

Fig. 17: Motor speeds at $\omega_{ref} = 5$ rpm, $\sigma_{R^2} = 0.3^2$.

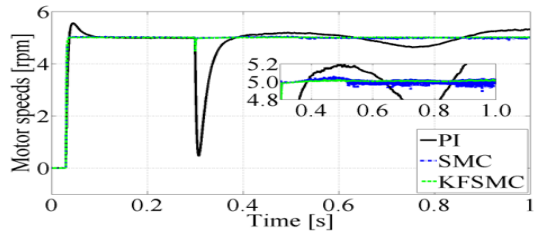

Fig. 18: Motor speeds at $\omega_{ref} = 5$ rpm, $\sigma_{R^2} = 0.5^2$.

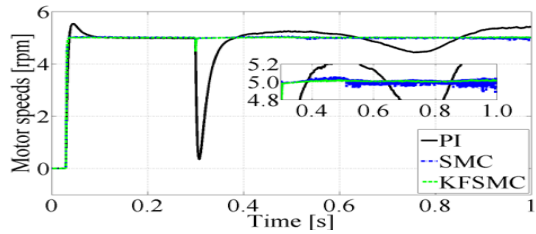

Fig. 19: Motor speeds at $\omega_{ref} = 5$ rpm, $\sigma_{R^2} = 0.7^2$.

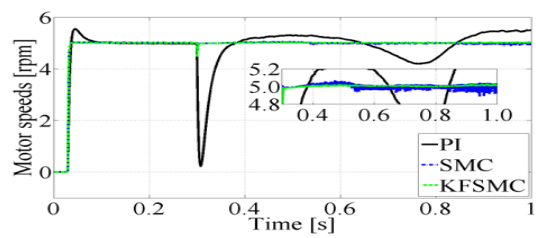

Fig. 20: Motor speeds at $\omega_{ref} = 5$ rpm, $\sigma_{R^2} = 0.9^2$.

tively. The main reason for this is that KF-SMC structure brings much lower overshoot and undershoot than PI one: overshoots and undershoots for KFSMC are respectively 2.29%-31.05% (see Tab. 3) and 9.84%-14.24% (see Tab. 4) of ones for PI. In comparison to SMC, overshoots and undershoots for KFSMC are respectively 32.09%-100.07% (see Tab. 3) and 97.30%-106.63% (see Tab. 4) of ones for SMC. Although many values are larger than 100%, but ripples of speed responses at duration 0.4 s – 1.0 s (see extractions in Figs. 6-20) for KFSMC are significantly smaller than ones for SMC, especially at reference speeds of 50 rpm and 5 rpm. This advantage is due to smoothing ability of Kalman filter in load estimation. For further analysis, Tabs. 5-6 list settling times.

In case of ω_{ref}= 500 rpm, settling times for all structures are almost the same. At $\omega_{ref} = 50$ rpm, SMC and KFSMC structures own approximately the same settling times, and they respec-

Tab. 2: ITAE value.

ω_{ref}	σ_{R^2}	PI	SMC	KFSMC
500	0.1^2	4.1042	4.0253	4.0176
	0.3^2	4.2044	4.0229	4.0152
	0.5^2	4.3138	4.0260	4.0186
	0.7^2	4.4181	4.0187	4.0117
	0.9^2	4.5419	4.0252	4.0189
50	0.1^2	0.0761	0.0287	0.0216
	0.3^2	0.1223	0.0284	0.0215
	0.5^2	0.1703	0.0284	0.0217
	0.7^2	0.2208	0.0282	0.0215
	0.9^2	0.2762	0.0284	0.0217
5	0.1^2	0.0515	0.0080	0.0042
	0.3^2	0.0847	0.0081	0.0042
	0.5^2	0.1186	0.0084	0.0043
	0.7^2	0.1538	0.0086	0.0044
	0.9^2	0.1910	0.0088	0.0046

Tab. 3: Overshoot [rpm].

ω_{ref}	σ_{R^2}	PI	SMC	KFSMC
500	0.1^2	0.9345	0.0818	0.0471
	0.3^2	0.8775	0.1094	0.1016
	0.5^2	0.8140	0.1537	0.1528
	0.7^2	0.7488	0.2015	0.1993
	0.9^2	0.7885	0.2447	0.2448
50	0.1^2	0.9331	0.0725	0.0286
	0.3^2	0.9231	0.0654	0.0294
	0.5^2	0.9123	0.0620	0.0358
	0.7^2	0.9016	0.0681	0.0440
	0.9^2	0.8916	0.0755	0.0535
5	0.1^2	0.5488	0.0457	0.0185
	0.3^2	0.5476	0.0434	0.0162
	0.5^2	0.5554	0.0421	0.0152
	0.7^2	0.5399	0.0405	0.0134
	0.9^2	0.5497	0.0392	0.0126

Tab. 4: Undershoot [rpm].

ω_{ref}	σ_{R^2}	PI	SMC	KFSMC
500	0.1^2	4.1980	0.6056	0.5979
	0.3^2	4.0875	0.5549	0.5473
	0.5^2	3.9849	0.4993	0.4939
	0.7^2	3.9049	0.4453	0.4333
	0.9^2	3.8310	0.3857	0.3769
50	0.1^2	4.2094	0.4595	0.4900
	0.3^2	4.1026	0.4497	0.4783
	0.5^2	4.0006	0.4371	0.4620
	0.7^2	3.9011	0.4226	0.4467
	0.9^2	3.8016	0.4091	0.4323
5	0.1^2	4.3010	0.4822	0.4977
	0.3^2	4.4163	0.4927	0.5031
	0.5^2	4.5348	0.5013	0.5174
	0.7^2	4.6585	0.5114	0.5257
	0.9^2	4.7858	0.5258	0.5356

Tab. 5: Settling times t_{s1} [s].

ω_{ref}	σ_{R^2}	PI	SMC	KFSMC
500	0.1^2	0.2049	0.2049	0.2049
	0.3^2	0.2048	0.2048	0.2048
	0.5^2	0.2048	0.2048	0.2048
	0.7^2	0.2047	0.2046	0.2047
	0.9^2	0.2048	0.2047	0.2048
50	0.1^2	0.0509	0.0487	0.0487
	0.3^2	0.0508	0.0486	0.0486
	0.5^2	0.0509	0.0486	0.0486
	0.7^2	0.0507	0.0484	0.0484
	0.9^2	0.0508	0.0485	0.0485
5	0.1^2	0.0786	0.0346	0.0347
	0.3^2	0.0781	0.0344	0.0345
	0.5^2	0.0786	0.0344	0.0345
	0.7^2	0.0771	0.0341	0.0342
	0.9^2	0.0777	0.0342	0.0342

tively bring 2.2-2.3 ms, 31.9-34.5 ms shorter in t_{s1}, t_{s2} than PI structure, there is not even t_{s2} in case of σ_{R^2}=0.9^2.

For lowest reference speed ω_{ref}= 5 rpm, before load activation (see Tab. 5), SMC and KFSMC structures give the same t_{s1} and dedicate 42.8-44.2ms less in t_{s1} than PI one. At this reference, after load activation (see Tab. 6), t_{s2} for PI structure exists only at $\sigma_{R^2} = 0.1^2$ and it is 68.4, 68.6ms respectively longer than that for SMC, KFSMC structures. At $\sigma_{R^2} = 0.3^2$, KFSMC gives a bit longer t_{s2} than SMC. In cases of $\sigma_{R^2} = \{0.5^2, 0.7^2, 0.9^2\}$, KFSMC still maintains t_{s2} while SMC brings much longer t_{s2}. The advantage once again shows noise-reduction ability of Kalman filter in load estimation (see Figs. 21-23), especially at ω_{ref} = 5 rpm (see Fig. 23).

However, trend of oscillation is increasing especially after load activation at ω_{ref} = 5 rpm (see Fig. 23). Reason of this is that high stator resistance uncertainty σ_{R^2}= 0.92 makes estimated values of components of stator flux vector (see Eqs. (12)-(13)) more and more inaccurate (see Figs. 24-25) although stator currents were

Tab. 6: Settling times t_{s2} [s].

ω_{ref}	σ_{R^2}	PI	SMC	KFSMC
500	0.1^2	0.3000	0.3000	0.3000
	0.3^2	0.3000	0.3000	0.3000
	0.5^2	0.3000	0.3000	0.3000
	0.7^2	0.3000	0.3000	0.3000
	0.9^2	0.3000	0.3000	0.3000
50	0.1^2	0.3345	0.3000	0.3000
	0.3^2	0.3336	0.3000	0.3000
	0.5^2	0.3327	0.3000	0.3000
	0.7^2	0.3319	0.3000	0.3000
	0.9^2	1.0000	0.3000	0.3000
5	0.1^2	0.3707	0.3021	0.3023
	0.3^2	1.0000	0.3022	0.3024
	0.5^2	1.0000	0.9561	0.3024
	0.7^2	1.0000	0.9953	0.3024
	0.9^2	1.0000	0.9579	0.3025

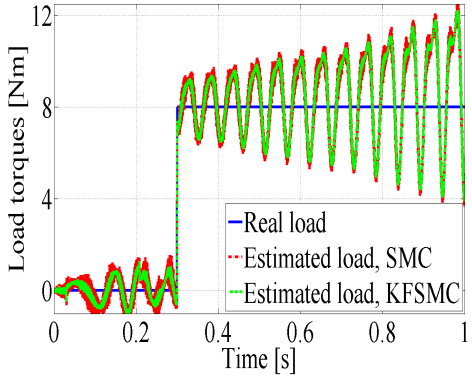

Fig. 21: Load and its estimates at $\omega_{ref} = 500$ rpm, $\sigma_{R^2} = 0.9^2$.

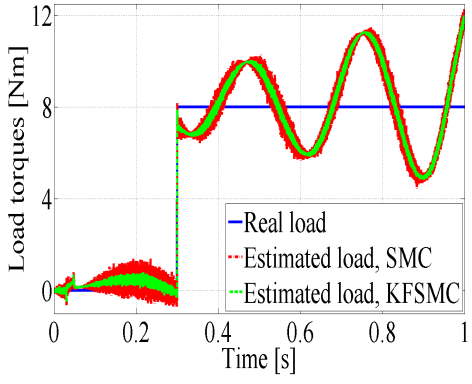

Fig. 22: Load and its estimates at $\omega_{ref} = 50$ rpm, $\sigma_{R^2} = 0.9^2$.

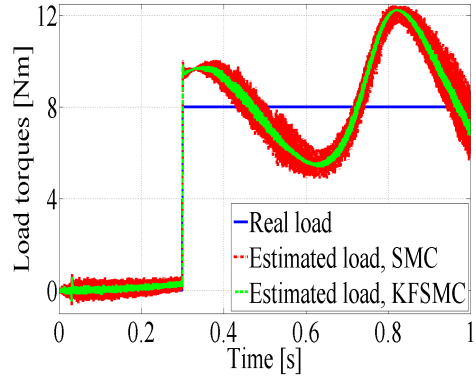

Fig. 23: Load and its estimates at $\omega_{ref} = 5$ rpm, $\sigma_{R^2} = 0.9^2$.

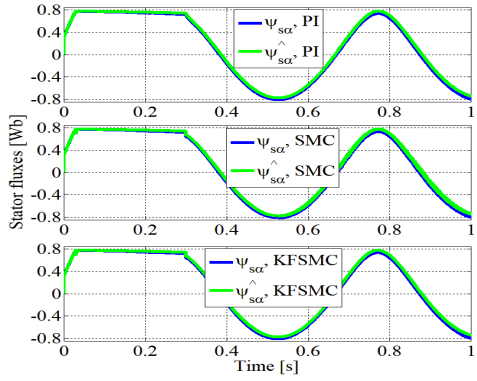

Fig. 24: Stator fluxes at $\omega_{ref} = 5$ rpm, $\sigma_{R^2} = 0.9^2$.

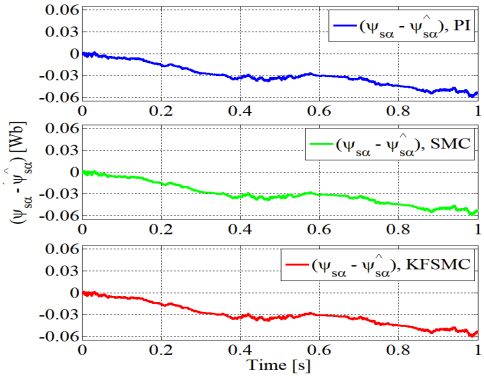

Fig. 25: Difference between stator flux and its estimated value at $\omega_{ref} = 5$ rpm, $\sigma_{R^2} = 0.9^2$.

Kalman filtered (see Fig. 26). The significant difference between stator flux and its estimated values leads to increasing errors in motor torque and load torque estimates (see Eqs. (16) & (28)). Another method that is less dependent on stator

resistance can be utilized to improve the accuracy of the estimates.

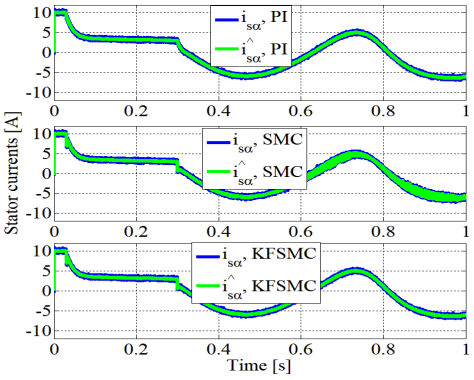

Fig. 26: Stator currents at $\omega_{ref} = 5$ rpm, $\sigma_{R^2} = 0.9^2$.

4. Conclusions

Drive structure using SMC and Kalman filtered load estimation was presented in the paper. Simulations were implemented at different reference speeds with wide ranges of noise variances of stator resistance. Proposed drive structure guaranteed system's Lyapunov stability, provided robustness to high uncertainty of stator resistance, and reduce chattering-phenomenon. It dedicated lower ITAE performance index than both the conventional and the SMC without Kalman filtration in load estimation ones, especially at lowest reference speed with ITAE value reduced by 91.8%-97.6% compared to conventional structure. Kalman Filter in its load estimate significantly reduced chattering problem compared to the one without Kalman Filter. The structure brought lower ripples at steady state, more robust settling times than two other ones. High-order or super-twisting or non-reaching phase, chattering-phenomenon free sliding mode control techniques can be used to obtain more robust speed controller, and approaches that are less dependent on stator resistance uncertainty can be employed to provide more accurate load torque estimates. Proposed approach can be utilized in robust sensorless control of IM drive.

References

[1] Hasse, K. (1969). Zur Dynamik Drehzahlgeregelter Antriebe mit stromrichtergespeisten Asynchronkurschlusslaüfer Maschinen. *Ph.D. dissertation, Technical University of Darmstadt, Darmstadt, Germany*, 1969.

[2] Blaschke, F. (1972). The Principle of Field Orientation as Applied to the New Transvektor Closed–Loop Control System for Rotating-Field Machines. *Siemens Review*, 34, 217-220.

[3] Tran, T.C., Brandstetter, P., Vo, H.H. (2019). The Sensorless Speed Controller of Induction Motor in DFOC Model Based on the Voltage and Current. *Journal of Advanced Engineering and Computation*, 3(1), 320-328.

[4] Takahashi, I. & Noguchi, T. (1986). A New Quick-Response and High-Efficiency Control Strategy of an Induction Motor. *IEEE Transactions on Industry Applications*, IA-22, 820-827.

[5] Depenbrock, M. (1988). Direct Self-Control (DSC) of Inverter-Fed Induction Machine. *IEEE Transactions on Power Electronics*, 3(4), 420-429.

[6] Vo, H. H., Nguyen, D.Q., Nguyen, Q.T., Dong, C.S.T., Tran, T.C., Brandstetter, P. (2021). Pulse-Width Modulation Direct Torque Control Induction Motor Drive with Kalman Filter. *Telkomnika*, 19(1), 277-284.

[7] O'Dwyer, A. (2009). Handbook of PI and PID Controller Tuning Rules. *Imperial College Press.*

[8] Vo, H.H. (2018). Fast Stability Analysis for Proportional-Integral Controller in Interval Systems. *Journal of Advanced Engineering and Computation*, 2(2), 111-120.

[9] Hsu, C. (2019). Fractional Order PID Control for Reduction of Vibration and Noise on Induction Motor. *IEEE Transactions on Magnetics*, 55(11), 1-7.

[10] Safaei, M. & Tavakoli, S. (2020). Improved PID Tuning Rules Using Fractional Calculus. *Proceedings of the 2020 28th Iranian Conference on Electrical Engineering (ICEE), Tabriz, Iran*, 1-5.

[11] Hekimoğlu, B., Ekinci, S. & Kaya, S. (2018). Optimal PID Controller Design of DC-DC Buck Converter using Whale Optimization Algorithm. *Proceedings of the 2018 International Conference on Artificial Intelligence and Data Processing (IDAP), Malatya, Turkey*, 1-6.

[12] Mukhtar, A., Tayal, V.K. & Singh, H. (2019). PSO Optimized PID Controller Design for the Process Liquid Level Control. *Proceedings of the 2019 3rd International Conference on Recent Developments in Control, Automation & Power Engineering (RDCAPE), Noida, India*, 590-593.

[13] Moura, J.P.de., Neto, J.V.d.F. & Rêgo, P.H.M. (2020). A Neuro-Fuzzy Model for Online Optimal Tuning of PID Controllers in Industrial System Applications to the Mining Sector. *IEEE Transactions on Fuzzy Systems*, 28(8), 1864-1877.

[14] Puchta, E.D.P., Siqueira, H.V. & Kaster, M.d.S. (2020). Optimization Tools Based on Metaheuristics for Performance Enhancement in a Gaussian Adaptive PID Controller. *IEEE Transactions on Cybernetics*, 50(3), 1185-1194.

[15] Negm, M.M.M., Bakhashwain, J.M. & Shwehdi, M.H. (2006). Speed Control of a Three-Phase Induction Motor Based on Robust Optimal Preview Control Theory. *IEEE Transactions on Energy Conversion*, 21(1), 77-84.

[16] Duda, T. & Vítecek, A. (2012). Robust Control Algorithms in Vector Oriented Control of Induction Motor. *Proceedings of the 13th International Carpathian Control Conference (ICCC), Ilmenau, Germany*, 137-140.

[17] Accetta, A., Alonge, F., Cirrincione, M., D'Ippolito, F., Pucci, M., Rabbeni, R. & Sferlazza, A. (2019). Robust Control for High Performance Induction Motor Drives Based on Partial State-Feedback Linearization. *IEEE Transactions on Industry Applications*, 55(1), 490-503.

[18] Safaeian, M., Jalilvand, A. & Taheri, A. (2021). Robust Control of Induction Motor in Presence of Disturbance. *Proceedings of the 2021 7th International Conference on Control, Instrumentation and Automation (ICCIA), Tabriz, Iran*, 1-5.

[19] Shtessel, Y., Edwards, C., Fridman, L., Levant, A. (2014). Sliding Mode Control and Observation. *Birkhäuser Basel.*

[20] Wadoo, A. (2013). Sliding Mode Control of Crowd Dynamics. *IEEE Transactions on Control Systems Technology*, 21(3), 1008-1015.

[21] Pradhan, R. & Subudhi, B. (2016). Double Integral Sliding Mode MPPT Control of a Photovoltaic System. *IEEE Transactions on Control Systems Technology*, 24(1), 285-292.

[22] Zhang, Q., Zhang, J. & Wang, Y. (2019). Sliding-Mode Control for Singular Markovian Jump Systems With Brownian Motion Based on Stochastic Sliding Mode Surface. *IEEE Transactions on Systems, Man, and Cybernetics: Systems*, 49(3), 494-505.

[23] Huynh-Van, V. & Tran-Thanh, P. (2019). Discrete Sliding Mode Control Design for Piezoelectric Actuator. *Journal of Advanced Engineering and Computation*, 3(3), 492-592.

[24] Yang, R. & Zheng, W.X. (2019). Two-Dimensional Sliding Mode Control of Discrete-Time Fornasini–Marchesini Systems. *IEEE Transactions on Automatic Control,* 64(9), 3943-3948.

[25] Dong, C., Brandstetter, P., Vo, H.H., Tran, T.C. & Vo, D.H. (2017). Adaptive Sliding Mode Controller for Induction Motor. *Proceedings of the AETA 2016: Recent Advances in Electrical Engineering and Related Sciences, Busan, Korea*, 543-553.

[26] Zhou, M., Feng, Y., Yu, X. & Han, F. (2017). Gain Margin Technique Based Continuous Sliding-Mode Control of Induction Motors. *Proceedings of the 2017 IEEE International Conference on Systems, Man, and Cybernetics (SMC), Banff, AB, Canada*, 2209-2212.

[27] Alonge, F., Cirrincione, M., D'Ippolito, F., Pucci, M. & Sferlazza, A. (2017). Robust Active Disturbance Rejection Control of Induction Motor Systems Based on Additional Sliding-Mode Component. *IEEE Transactions on Industrial Electronics*, 64(7), 5608-5621.

[28] Mishra, J., Wang, L., Zhu, Y., Yu, X. & Jalili, M. (2019). A Novel Mixed Cascade Finite-Time Switching Control Design for Induction Motor. *IEEE Transactions on Industrial Electronics*, 66(2), 1172-1181.

[29] Bose, B. K. (2002). Modern Power Electronics and AC Drives. *Prentice Hall.*

About Authors

Hau Huu VO hold a PhD degree from Technical University of Ostrava (VSB-TUO), Czech Republic in 2017. He has been working as a Lecturer at Faculty of Electrical and Electronics Engineering (FEEE), Ton Duc Thang University (TDTU). He has published 10 conference papers and 8 journal papers. His current research interests are intelligent electrical drives.

Dat Vinh Phat TRAN received his BEng degree in Automation and Control Engineering from FEEE, TDTU in 2018. He is now a Master Student at the same faculty. His research interests include applications of robust control in electrical drives, and building automation

Tri Quang THIEU hold his MSc degree from Asian Institute of Technology in 2009. He has been working as a Lecturer at FEEE, TDTU. His research interests include robotics, metrology, and electrical drives.

Anh Tuan LE completed his PhD degree at Dayeh University, Taiwan in 2016. He works as a Lecturer at FEEE, TDTU, Vietnam. He has published 4 conference papers and 4 journal papers. His research interests are applications of Kalman filter and sliding mode control in vehicle control systems.

Chau Si Thien DONG received her PhD degree from VSB-TUO, Czech Republic in 2017. She is now dean of FEEE, TDTU, Vietnam. She has published 15 conference papers and 8 journal papers. Her research interests focus on robust controllers and observers of AC drives.

Pavel BRANDSTETTER received his PhD degree at Brno University in 1987. He is now full professor and dean of Faculty of Electrical Engineering and Computer Science at VSB-TUO, Czech Republic. He has published more than 65 conference papers and 30 journal papers. His research interests are intelligent methods in electrical drives and power electronics.